Hopf bifurcations to quasi-periodic solutions for the two-dimensional Poiseuille flow

By PABLO S. CASAS[1] AND ÀNGEL JORBA[2]

[1]Departamento de Matemática Aplicada I, Universidad Politécnica de Cataluña
Diagonal, 647; 08028 Barcelona. Spain. e-mail: pablo@casas.upc.es

[2]Departamento de Matemática Aplicada y Análisis, Universidad de Barcelona,
Gran Via, 585; 08007 Barcelona. Spain. e-mail: angel@maia.ub.es

This paper studies various Hopf bifurcations in the two-dimensional Poiseuille problem. For several values of the wavenumber α, we obtain the branch of periodic flows which are born at the Hopf bifurcation of the laminar flow. It is known that, taking $\alpha \approx 1$, the branch of periodic solutions has several Hopf bifurcations to quasi-periodic orbits. For the first of them, previous calculations seem to indicate that the bifurcating quasi-periodic flows are stable and go backwards with respect to the Reynolds number Re. By improving the precision of those previous works we find that the bifurcating flows are unstable and go forward with respect to Re. We have also analysed the second Hopf bifurcation of periodic orbits for $\alpha \approx 1$ to find again quasi-periodic solutions with increasing Re. In this case they are stable to superharmonic disturbances.

The proposed numerical scheme is based on a full numerical integration of the Navier-Stokes equations and the use of suitable Poincaré sections. The most intensive part of the computations has been done in parallel. We believe that this methodology can also be applied to similar problems.

1. Introduction

The theory of hydrodynamic stability is one of the main topics in fluid mechanics. Poiseuille as well as Taylor–Couette flow are test problems where it is possible the evaluation of different analytical and numerical methods, due essentially to the simplicity of their geometry. The dynamics of Poiseuille flow departs from the laminar flow. Its stability to infinitesimal disturbances has been analysed linearly, which gives rise to the Orr–Sommerfeld equation. This equation has been studied by several authors as Thomas (1953), Orszag (1971), and Maslowe (1985) among others, and it is well understood. The critical Reynolds number of the linear theory, $Re_{cr} = 5772.22$ for the wavenumber $\alpha = 1.02056$, has been obtained by this approach. However, as experiments of Carlson, Widnall & Peeters (1982), Nishioka & Asai (1985), and Alavyoon, Henningson & Alfredsson (1986) showed, transition to turbulence is observed for Reynolds number ≈ 1000, what motivates that finite-amplitude disturbances originate the transition. The understanding of the transition to turbulence has been conjectured by Saffman (1983) to depend on intermediate vortical states and turbulence takes place due to their three-dimensional instability. Examples of vortical states are periodic flows in time or space, among which can be mentioned: two-dimensional travelling waves, secondary flows in two or three dimensions (for them the flow rate and the pressure gradient are constants) and quasi-periodic solutions. Ehrenstein & Koch (1991) discovered a new family of secondary bifurcation branches in dimension 3 which contains only even spanwise Fourier modes and it reduces the critical Reynolds number to $Re_{Q_m} \approx 1000$ (defined in terms of the averaged velocity across the channel) as observed in experiments.

Two-dimensional disordered motion is associated with the large scales of some turbulent flows, so there probably exist attractors for those two-dimensional flows. Besides, two-dimensional and three-dimensional states can compete and coexist in the final flow (cf. Jiménez 1987, and the references therein). In spite of the fact that transition to turbulence is a three-dimensional phenomenon, there are many properties of the two-dimensional flows observed in fully turbulent three-dimensional flows such as wall sweeps, ejections, intermittency and bursting, as Jiménez (1990) showed. The two-dimensional case has attracted the attention of many authors but it is not completely understood as the problem of two-dimensional transition to turbulence proves. Due to Squire's (1933) theorem to every three-dimensional perturbation of the linearized Navier–Stokes equations for a given Re, α, it corresponds a two-dimensional one for some $\tilde{\alpha} \geqslant \alpha$ and $\tilde{Re} \leqslant Re$, so the critical Re for the linear theory must be attained by a two-dimensional flow. This result has been one of the main reasons to firstly try to understand the two-dimensional case, apart from the obvious easiness of computations compared to the three-dimensional situation. In addition, some of the properties obtained from the two-dimensional case can also provide new insight for three-dimensional flows.

In this work we try to analyse the dynamics of an easily treatable problem without domain complexities as is the case of the two-dimensional Poiseuille flow. Different levels of bifurcation to respective vortical states are considered, starting at the basic parabolic flow. From this flow, a family of travelling waves is born subcritically. There are many papers concerning this kind of waves. Soibelman & Meiron (1991) gave an excellent review about it. We also reproduce the calculations to find the travelling waves for several values of α. Jiménez (1987, 1990) and Soibelman & Meiron (1991) obtained the next level of bifurcation to quasi-periodic solutions. Employing full numerical simulation on time Jiménez (1987, 1990) computed different attractor flows with a moderate number of Chebyshev and Fourier modes. On the other hand Soibelman & Meiron (1991) implemented an algebraic approach to capture stable and unstable quasi-periodic flows, but the number of modes used were not enough to give good results and they were not able to carry out the stability analysis. The method implemented in the present work combines both: We solve a stationary problem to compute travelling waves when the observer is moving with an appropriate speed, whereas the quasi-periodic flows are found by means of full numerical integration of the Navier–Stokes equations. We have needed a Poincaré section of the flow in order to obtain also unstable quasi-periodic solutions. These unstable intermediate states of the flow provide a highly useful insight into the transition process, as exemplified by secondary bifurcations in shear flows. The quasi-periodic solutions found correspond to the first two Hopf bifurcations of travelling waves. The property of behaving as time-periodic flows if we take an appropriate Galilean reference, simplifies enormously the search of this kind of solutions. In this case, the associated period on time is $O(10000)$ at the first Hopf bifurcation, what makes its temporal integration very costly. The employed numerical procedure utilizes a parallel algorithm to evaluate the different columns of a Jacobian matrix, needed in the application of Newton's method. We find that on the two first Hopf bifurcations, there exist quasi-periodic flows with increasing Re, so the bifurcations are both supercritical. For the first bifurcation all the quasi-periodic solutions found are unstable but for the second one they are stable to disturbances with the same wavenumber α.

Once we have situated the different studies concerning Poiseuille flow, in the next section we pose the concrete terms that define the problem in two-dimensional, together with their equations. Next in § 3 we give the details of the numerical method. In § 4 we review some results of the Orr–Sommerfeld equation and obtain, for several values of α, the bifurcating solutions of time-periodic flows. From these we analyse in § 5 the bifurcating branches to quasi-periodic solutions at the two first Hopf bifurcations. Finally in § 6 we point out some conclusions.

2. Poiseuille flow

We consider the flow of a viscous incompressible two-dimensional fluid, in a channel between two parallel walls, governed by the Navier–Stokes equations together with the incompressibility condition

$$\rho\left[\frac{\partial \mathbf{u}}{\partial t}+(\mathbf{u}\cdot\boldsymbol{\nabla})\mathbf{u}\right]=-\nabla p+\mu\Delta\mathbf{u},\qquad \boldsymbol{\nabla}\cdot\mathbf{u}=0,$$

where $\mathbf{u}=\mathbf{u}(x,y,t)=(u,v)(x,y,t)$, are the components of the velocity, $p=p(x,y,t)$ the pressure and ρ,μ the constant density and viscosity respectively. As boundary conditions we suppose no-slip on the channel walls at $y=\pm h$ and, at artificial boundaries in the stream direction x, a period L, i.e.

$$\left.\begin{array}{r}u(x,\pm h,t)=v(x,\pm h,t)=0\\ (u,v,p')(x+L,y,t)=(u,v,p')(x,y,t)\end{array}\right\}\qquad x\in\mathbb{R},\quad y\in[-h,h],\quad t\geqslant 0,$$

being $p-p'=-Gx$, where $-G$ is an imposed constant pressure gradient which drives the flow in the streamwise direction. For this system there is a time-independent solution known as the basic or laminar flow that has a parabolic profile, namely

$$u_b(y)=U_c\left[1-\left(\frac{y}{h}\right)^2\right],\quad v_b=0,\quad \nabla p_b=(-G,0),$$

being $U_c=Gh^2/(2\mu)$. According to this condition, we define the Reynolds number Re in terms of the channel half-length h and the centre velocity U_c of the basic flow and thus $Re=Gh^3\rho/(2\mu^2)$. Rescaling time t, lengths x,y, velocities u,v and pressure p we obtain the Navier–Stokes equations in adimensional form

$$\frac{\partial \mathbf{u}}{\partial t}+(\mathbf{u}\cdot\boldsymbol{\nabla})\mathbf{u}=-\nabla p+\frac{1}{Re}\Delta\mathbf{u},\qquad \boldsymbol{\nabla}\cdot\mathbf{u}=0,\tag{2.1}$$

with analogous boundary conditions

$$\left.\begin{array}{r}u(x,\pm 1,t)=v(x,\pm 1,t)=0\\ (u,v,p')(x+L,y,t)=(u,v,p')(x,y,t)\end{array}\right\}\qquad x\in\mathbb{R},\quad y\in[-1,1],\quad t\geqslant 0,\tag{2.2}$$

(p' the pressure deviation as above), and whose basic flow is now written as

$$u_b(y)=1-y^2,\quad v_b=0,\quad \nabla p_b=(-\frac{2}{Re},0),$$

where for convenience we have used the same notation for adimensional magnitudes. Making use of the spatial symmetry due to artificial boundaries at x and $x+L$, we consider equations (2.1) viewed by an observer who is moving at certain speed c and accordingly we perform the change of variable $\tilde{x}=x-ct$ in system (2.1) which (writing again x instead of $\tilde{x}$) becomes

$$\left\{\begin{aligned} \frac{\partial u}{\partial t}+(u-c)\frac{\partial u}{\partial x}+v\frac{\partial u}{\partial y} &= -\frac{\partial p}{\partial x}+\frac{1}{Re}\left(\frac{\partial^2 u}{\partial x^2}+\frac{\partial^2 u}{\partial y^2}\right)\\ \frac{\partial v}{\partial t}+(u-c)\frac{\partial v}{\partial x}+v\frac{\partial v}{\partial y} &= -\frac{\partial p}{\partial y}+\frac{1}{Re}\left(\frac{\partial^2 v}{\partial x^2}+\frac{\partial^2 v}{\partial y^2}\right)\\ \frac{\partial u}{\partial x}+\frac{\partial v}{\partial y} &= 0, \end{aligned}\right. \tag{2.3}$$

together with boundary conditions as in (2.2). We can recover (2.1) by simply taking $c=0$ in (2.3).

3. Numerical approach

For system (2.3) we want to follow the temporal evolution of an initial flow subjected to the incompressibility condition, $\boldsymbol{\nabla}\cdot\mathbf{u}=0$, and boundary conditions (2.2). To this end we use a spectral method to approximate velocities u, v and pressure deviation p'. Since we suppose u, v, p' periodic in x, we replace them by their Fourier series (with $\alpha = 2\pi/L$ the parameter wavenumber) truncated at some positive integer N:

$$(u,v,p')(x,y,t)=\sum_{k=-N}^{N}(\hat{u}_k,\hat{v}_k,\hat{p}_k)(y,t)\mathrm{e}^{\mathrm{i}k\alpha x}, \qquad x\in\mathbb{R}, \quad y\in[-1,1], \quad t\geqslant 0,$$

which substituted in system (2.3) gives rise to a system of partial differential equations for the Fourier coefficients $(\hat{u}_k,\hat{v}_k,\hat{p}_k)$,

$$\left\{\begin{aligned} \frac{\partial \hat{u}_k}{\partial t}+\left[\widehat{(u-c)\frac{\partial u}{\partial x}+v\frac{\partial u}{\partial y}}\right]_k &= -\mathrm{i}k\alpha\hat{p}_k+\frac{1}{Re}\left(-k^2\alpha^2\hat{u}_k+\frac{\partial^2\hat{u}_k}{\partial y^2}\right)+\delta_{k0}G\\ \frac{\partial \hat{v}_k}{\partial t}+\left[\widehat{(u-c)\frac{\partial v}{\partial x}+v\frac{\partial v}{\partial y}}\right]_k &= -\frac{\partial \hat{p}_k}{\partial y}+\frac{1}{Re}\left(-k^2\alpha^2\hat{v}_k+\frac{\partial^2\hat{v}_k}{\partial y^2}\right)\\ \mathrm{i}k\alpha\hat{u}_k+\frac{\partial \hat{v}_k}{\partial y} &= 0, \end{aligned}\right. \tag{3.1}$$

where $-N\leqslant k\leqslant N$, $\widehat{[\cdot]}_k$ stands for the order kth Fourier coefficient of $[\cdot]$, $\delta_{00}=1$, and $\delta_{k0}=0$ for $k\neq 0$. Because u, v, p' are supposed to be real functions, it is enough to consider modes $\hat{u}_k, \hat{v}_k, \hat{p}_k$ for $k=0,\ldots,N$ in equations (3.1). The corresponding no slip boundary conditions in (2.2) are now written as

$$(\hat{u}_k,\hat{v}_k)(\pm 1,t)=0, \quad \text{for } t\geqslant 0 \text{ and } k=0,\ldots,N. \tag{3.2}$$

To get rid of derivatives in the transversal variable y we employ the collocation method, in which every equation is imposed at selected (collocation) points: we have chosen the Chebyshev abscissas because of their good convergence properties and the possibility of utilizing fast Fourier transforms. In this way we suppose

$$\hat{u}_k(y,t)=\sum_{j=0}^{M}\tilde{u}_{kj}(t)T_j(y), \quad \hat{v}_k(y,t)=\sum_{j=0}^{M}\tilde{v}_{kj}(t)T_j(y), \quad \hat{p}_k(y,t)=\sum_{j=0}^{M-1}\tilde{p}_{kj}(t)T_j(y),$$

for $k=0,\ldots,N$, approximated by Chebyshev polynomials $T_j(y)=\cos(j\arccos(y))$ for $j=0,\ldots,M$, being M a positive integer. We consider their respective values $\hat{u}_{km}(t)=$

$\hat{u}_k(y_m,t)$, $\hat{v}_{km}(t)=\hat{v}_k(y_m,t)$ on Chebyshev abscissas $y_m=\cos(\pi m/M)$ for $m=1,\dots,M-1$, whereas for $\hat{p}_k(y,t)$ we take its value $\hat{p}_{km}(t)=\hat{p}_k(y_{m+1/2},t)$ at the staggered grid $y_{m+1/2}=\cos(\pi(m+1/2)/M)$ for $m=0,\dots,M-1$.

Momentum equations in (3.1) are enforced on the first grid, y_m, whereas the second one, $y_{m+1/2}$, is taken for the continuity equation. If we used the same collocation points for the pressure and continuity equation as for the velocity and momentum equations, then we would obtain an undetermined linear system for the discrete dependent variables $\hat{u}_{km},\hat{v}_{km},\hat{p}_{km}$ (cf. Canuto *et al.* 1988). The boundary conditions (3.2) are imposed letting $\hat{u}_{k0}=\hat{u}_{kM}=\hat{v}_{k0}=\hat{v}_{kM}=0$. We change from one grid to the other by means of appropriate cosine transforms (and their respective inverses)

$$\begin{aligned} w_m &= \sum_{j=0}^{M}\tilde{w}_jT_j(y_m)=\sum_{j=0}^{M}\tilde{w}_j\cos\frac{\pi mj}{M}, \quad m=1,\dots,M-1, \quad \text{or} \\ w_m &= \sum_{j=0}^{M-1}\tilde{w}_jT_j(y_{m+\frac{1}{2}})=\sum_{j=0}^{M-1}\tilde{w}_j\cos\frac{\pi(2m+1)j}{2M}, \quad m=0,\dots,M-1, \end{aligned} \tag{3.3}$$

where w_m represents $\hat{u}_{km},\hat{v}_{km}$ or $\hat{p}_{km}$ for $k=0,\dots,N$ and $\tilde{w}_j$ their discrete Chebyshev coefficients.

To emphasize the linear character of some operations, we now write system (3.1) as

$$\dot{u}_k=-\left[(u-c)\frac{\partial u}{\partial x}+v\frac{\partial u}{\partial y}\right]_k-D_xC_1^{-1}C_2p_k+\frac{1}{Re}(D_x^2+C_1^{-1}D_y^2C_1)u_k+\delta_{k0}G \tag{3.4}$$

$$\dot{v}_k=-\left[(u-c)\frac{\partial v}{\partial x}+v\frac{\partial v}{\partial y}\right]_k-C_1^{-1}D_yC_2p_k+\frac{1}{Re}(D_x^2+C_1^{-1}D_y^2C_1)v_k \tag{3.5}$$

$$D_xC_2^{-1}C_1u_k+C_2^{-1}D_yC_1v_k=0, \tag{3.6}$$

for $k=0,\dots,N$, where we have taken '$\hat{\ }$' out of $\widehat{[\cdot]}_k,\hat{u}_k,\hat{v}_k,\hat{p}_k$ for convenience; these represent vectors of values at the grids y_m and $y_{m+1/2}$; C_1,C_2 are the matrices of respective cosines transforms defined in (3.3) and D_x,D_y denote the respective matrices of partial derivatives in x,y, so that $D_xu_k=\mathrm{i}k\alpha u_k$ and $D_y(\tilde{w}_0,\dots,\tilde{w}_M)^t$ represents the Chebyshev coefficients of the polynomial $\sum_{j=0}^{M}\tilde{w}_j(t)T_j'(y)$.

From (3.6) we obtain a matrix T_k that carries out the transformation $\bar{v}_k=T_k\bar{u}_k$ where $\bar{u}_k=(u_{k,1},\dots,u_{k,M-2})^t$ and $\bar{v}_k=(u_{k,M-1},v_{k,1},\dots,v_{k,M-1})^t$ for $k=1,\dots,N$. For $k=0$ we have $v_{0,1}=\dots=v_{0,M-1}=0$, seeing that, due to the continuity equation, $\partial v_0/\partial y=0$, and the boundary conditions, $v_0(\pm1)=0$, we get $v_0(y)=0$. If for $k=0,\dots,N$ we put

$$\begin{aligned} U_k &= -\left[(u-c)\frac{\partial u}{\partial x}+v\frac{\partial u}{\partial y}\right]_k+\frac{1}{Re}(D_x^2+C_1^{-1}D_y^2C_1)u_k+\delta_{k0}G \\ V_k &= -\left[(u-c)\frac{\partial v}{\partial x}+v\frac{\partial v}{\partial y}\right]_k+\frac{1}{Re}(D_x^2+C_1^{-1}D_y^2C_1)v_k, \\ \bar{D}_y &= \begin{pmatrix}(D_x)_{M-1}\\ D_y\end{pmatrix}, \quad \bar{V}_k=\begin{pmatrix}(U_k)_{M-1}\\ V_k\end{pmatrix}, \end{aligned}$$

from (3.5) and equation $M-1$ of (3.4) we may find

$$p_k=-(C_1^{-1}\bar{D}_yC_2)^{-1}(\dot{\bar{v}}_k-\bar{V}_k), \quad k=1,\dots,N \tag{3.7}$$

For $k=1,\dots,N$ and $m=1,\dots,M-2$ we substitute (3.7) in (3.4) to get $\dot{\bar{u}}_k=A_k(T_k\dot{\bar{u}}_k-V_k)+U_k$, being $A_k=D_xC_1^{-1}C_2(C_1^{-1}\bar{D}_yC_2)^{-1}$ and therefore we finally arrive at a system which only depends on u_0 and $\bar{u}_k$ for $k = 1, \ldots, N$, namely

$$\begin{cases} \dot{u}_0 = U_0 \\ \dot{\bar{u}}_k = (I - A_k T_k)^{-1}(U_k - A_k V_k), \quad k = 1, \ldots, N. \end{cases} \tag{3.8}$$

We remark that this last system does not depend on $\bar{v}_k$ and p_k for $k = 0, \ldots, N$.

In (3.8) it just remains to discretize temporal derivatives. We express it as

$$\dot{u} = \mathcal{L}(u) + \mathcal{N}(u), \tag{3.9}$$

where u stands for u_0 or $\bar{u}_k$ for $k = 1, \ldots, N$ and $\mathcal{L}(u), \mathcal{N}(u)$ corresponds to linear (pressure and viscosity) and nonlinear (advection) terms in u respectively on the right hand side of (3.8). We adopt a usual scheme for advection-diffusion problems: Letting u^n be u at the time instant $n\Delta t$ for some fix time step Δt, we approximate $\mathcal{N}(u)$ by an explicit method (Adams–Bashforth) and $\mathcal{L}(u)$ by an implicit one (Crank–Nicolson) and so (3.9) yields

$$u^{n+1} - \frac{\Delta t}{2}\mathcal{L}(u^{n+1}) = u^n + \frac{\Delta t}{2}\left[\mathcal{L}(u^n) + 3\mathcal{N}(u^n) - \mathcal{N}(u^{n-1})\right]. \tag{3.10}$$

Taking into account that in (3.8) u_0 has only real components but for $k = 1, \ldots, N$, $\bar{u}_k$ is a complex vector, we conclude that each time step it is solved a block diagonal linear system of total real dimension $(2N+1)(M-2)+1$. The block for $k = 0$ has dimension $M-1$ and $M-2$ for the $2N$ remaining blocks.

4. Periodic solutions

Before applying the previously described numerical scheme we make some considerations about the Orr–Sommerfeld equation and time-periodic solutions. Firstly, we can eliminate the pressure in the Navier–Stokes equations by applying the curl operator $(\boldsymbol{\nabla} \times \cdot)$ to the momentum equation in (2.1) to get

$$\frac{\partial \boldsymbol{\omega}}{\partial t} + \mathbf{u} \cdot \nabla \boldsymbol{\omega} - \boldsymbol{\omega} \cdot \nabla \mathbf{u} = \frac{1}{Re}\Delta \boldsymbol{\omega}, \tag{4.1}$$

being $\boldsymbol{\omega} = \boldsymbol{\nabla} \times (u, v, 0) = (0, 0, \omega)$ the vorticity vector in the plane case and $\omega = v_x - u_y$. The equation for ω, the third component of (4.1), is known as the vorticity equation and it is expressed as

$$\omega_t + \psi_y \omega_x - \psi_x \omega_y = \frac{1}{Re}\Delta \omega, \tag{4.2}$$

where $\psi = \psi(x, y, t)$ is the stream function which, due to the divergence free condition, can be found such that $\psi_x = -v$ and $\psi_y = u$. We separate the stream function as $\psi = \psi_b + \varepsilon\hat{\psi}$, where $\psi_b = \psi_b(y)$ is the stream function corresponding to the laminar flow, ε is a small parameter and $\hat{\psi} = \hat{\psi}(x, y, t)$ is a perturbation of ψ_b. Substituting ψ into (4.2), using that $\Delta\psi = -\omega$ and neglecting nonlinear terms in $\hat{\psi}$, we obtain the linearization of (4.2) as

$$\Delta\hat{\psi}_t + u_b \Delta\hat{\psi}_x - u_b''\hat{\psi}_x = \frac{1}{Re}\Delta^2\hat{\psi}. \tag{4.3}$$

If we substitute $\hat{\psi} = \exp(-\lambda t)\xi(x, y)$ in (4.3) then we obtain a spectral problem

$$-\lambda\Delta\xi + u_b \Delta\hat{\xi}_x - u_b''\hat{\xi}_x = \frac{1}{Re}\Delta^2\hat{\xi}. \tag{4.4}$$

Due to boundary conditions (2.2) we consider $\hat{\psi}$ a $2\pi/\alpha$-periodic function in x and thus we can write

$$\xi(x, y) = \sum_k \hat{\xi}_k(y) \mathrm{e}^{\mathrm{i}k\alpha x}.$$

Since (4.4) is a linear problem we may suppose that it is satisfied by each of the terms $\hat{\xi}_k(y)\mathrm{e}^{\mathrm{i}k\alpha x}$. Therefore, renaming $k\alpha$ as α, we impose (4.4) for $\xi = \phi(y)\mathrm{e}^{\mathrm{i}\alpha x}$ and so it gives

$$(u_b - c)(\phi'' - \alpha^2\phi) - u_b''\phi = \frac{1}{\mathrm{i}\alpha Re}(\phi^{(4)} - 2\alpha^2\phi'' + \alpha^4\phi), \tag{4.5}$$

an ordinary differential equation on ϕ, known as the Orr–Sommerfeld equation, where $c = -\mathrm{i}\lambda$. From (2.2) we have immediately $\phi(\pm 1) = \phi'(\pm 1) = 0$, as boundary conditions for ϕ, which together with (4.5) represent an eigenvalue problem for Re, α, c and the eigenfunction ϕ. In this way if $c = c_r + \mathrm{i}c_i$ is a complex eigenvalue with $c_i > 0$, then the laminar flow is unstable to small disturbances according to the linear theory.

We have employed finite differences to approximate $\phi(y)$ and its derivatives in an uniform mesh $\bar{y}_m = 2m/(n+1) - 1 \in [-1, 1]$ for $m = 0, \ldots, n+1$ and n positive integer sufficiently large. After substituting $\phi(\bar{y}_m)$, $m = 0, \ldots, n+1$ and the approximation to its derivatives in (4.5) we obtain an eigenvalue problem of finite dimension: $A\phi = cB\phi$, where A, B are matrices depending only on Re, α, and n. We solve it (by means of the power method) to get simply the eigenvalue with the largest imaginary part, that is to say, the most unstable one. We have obtained the known results reported by other authors, e.g. Orszag (1971). The neutral stability curve, where $c_i = 0$, is presented in figure 1. In this figure, each point in the Re–α plane represents a perturbation of the laminar solution whose stability is decided upon its position. We also observe the critical Reynolds number, $Re_{cr} = 5772.22$ for $\alpha = 1.02056$, so that if $Re < Re_{cr}$ the laminar solution is linearly stable for any value of α.

Next, we use the above results to look for periodic solutions on time. Due to the translational symmetry of the channel in x (the artificial boundaries in (2.2)), it is showed in Rand (1982) that if we have $u(x, y, t)$ such that

$$u(x, y, t+T) = u(x, y, t), \quad \text{for all } x \in \mathbb{R}, \quad y \in [-1, 1], \quad t \geqslant 0$$

and some $T > 0$ (or in other words, $u(x, y, t)$ is T-periodic on time), then it is a rotating (or travelling) wave, i.e.

$$u(x, y, t) = u(x - ct, y, 0), \quad \text{for } c = \frac{L}{T}. \tag{4.6}$$

Therefore $u(x, y, t)$ is observed as a stationary solution in a system of reference moving at speed c as in (2.3). This fact allows us to search for periodic solutions on time as functions $u(x, y)$ which solve the stationary version of (2.3) or, in its discretized form, the stationary version of (3.8)

$$\begin{cases} 0 = U_0 \\ 0 = (I - A_k T_k)^{-1}(U_k - A_k V_k), \quad k = 1, \ldots, N. \end{cases} \tag{4.7}$$

What we have in (4.7) is a zeros search problem for a system of nonlinear equations of dimension $(2N+1)(M-2)+1$ for the unknown Fourier coefficients $u_0, \bar{u}_1, \ldots, \bar{u}_N$. We solve it by means of Newton's method.

We need first an approximated solution of (4.7). With the numerical integrator (3.10) of system (2.3), we follow the temporal evolution of an initial flow close to the laminar solution. In this way we are able to check our results comparing with Re_{cr} computed in Orszag (1971). Taking $\alpha = 1.02056, Re > Re_{cr}$ and the laminar solution as initial

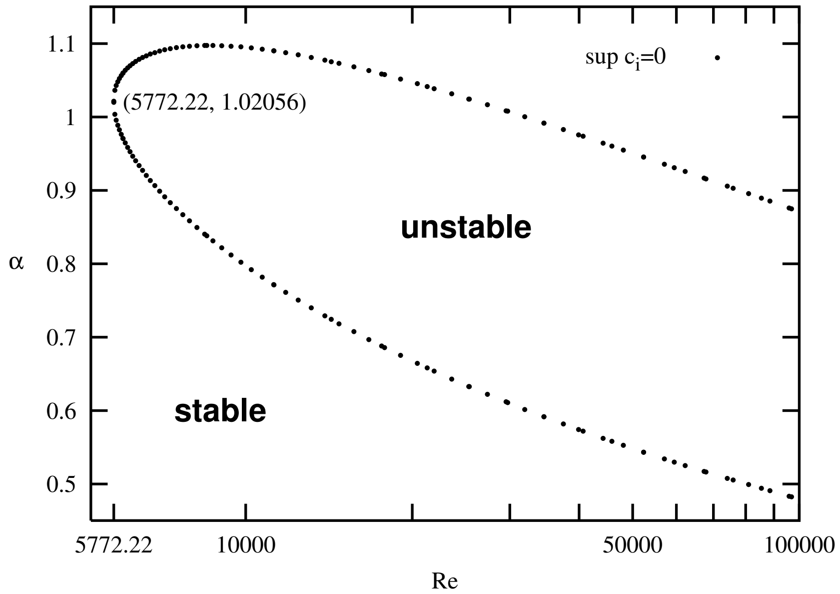

FIGURE 1. Neutral stability curve for the laminar solution. For each point in this curve the most unstable eigenvalue c is real. The critical Reynolds number is attained at $Re_{cr} = 5772.22$. The curve splits the Re-α plain in two stability regions as shown in the graph. For $\alpha \geqslant 1.1$ the laminar flow is linearly stable for every Re.

condition for (3.8), we observe how this solution is not stable, as it evolves to another steady flow which turns out to be T-periodic on time for some value of T. Up to errors of order $O((\Delta t)^2)$ (those of the time discretization (3.10)), this T-periodic solution satisfies (4.7) and it is thus a rotating wave. We improve its accuracy taking it as an initial guess for the Newton's method applied to (4.7).

If we use Re as a continuation parameter, we can trace a curve of periodic flows by solving (4.7) for each Reynolds number. This is implemented numerically by pseudo-arclength continuation. Given a profile of velocities (u, v) we define its amplitude A, as the distance to the laminar profile $(u_b, 0)$ in the L_2-norm

$$A = \frac{1}{2L}\|(u - u_b, v)\|_2, \qquad \|(u,v)\|_2^2 = \int_0^L \int_{-1}^1 \left[u(x,y)^2 + v(x,y)^2\right] \mathrm{d}y \, \mathrm{d}x.$$

For a rotating wave as defined in (4.6), its amplitude does not depend on time since for a fixed t

$$\begin{aligned}\int_0^L \int_{-1}^1 u(x,y,t)^2 \mathrm{d}y \, \mathrm{d}x &\stackrel{1}{=} \int_0^L \int_{-1}^1 u(x-ct,y,0)^2 \mathrm{d}y \, \mathrm{d}x \\ &\stackrel{2}{=} \int_{-ct}^{L-ct} \int_{-1}^1 u(\tilde{x},y,0)^2 \mathrm{d}y \, \mathrm{d}\tilde{x} \stackrel{3}{=} \int_0^L \int_{-1}^1 u(\tilde{x},y,0)^2 \mathrm{d}y \, \mathrm{d}\tilde{x}.\end{aligned} \tag{4.8}$$

In step 1 we apply definition (4.6). For step 2 we make the change of variable $\tilde{x} = x - ct$, and because u, v are L-periodic in x we have step 3.

We notice that zeros of system (4.7) can either correspond to stable or unstable time-periodic solutions. With a stable solution it is meant the one for which any small disturbance ultimately decays to zero, whereas if some of those disturbances remain permanently away from zero, it is called unstable.

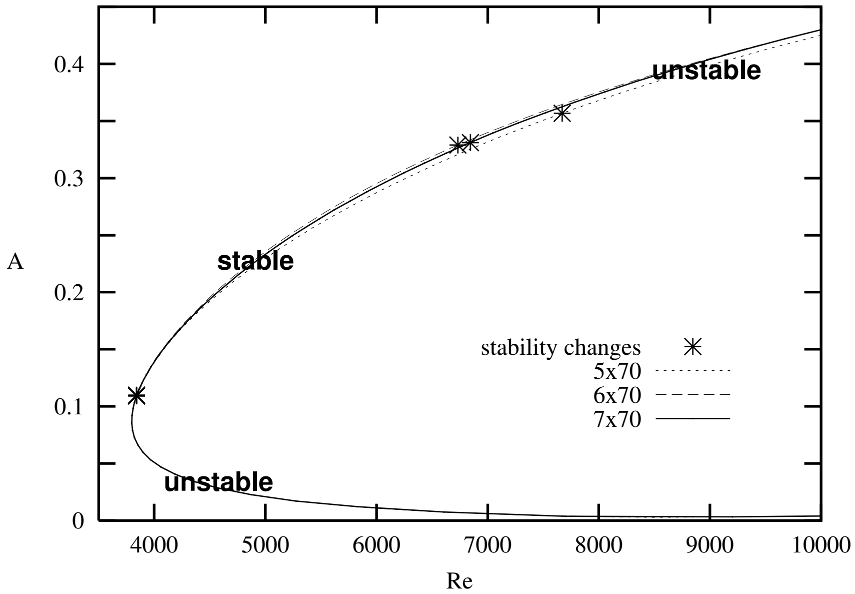

FIGURE 2. Bifurcating curve of periodic flows for several discretizations specified as $N \times M$, and $\alpha = 1.1$. On each curve there are two '*' corresponding to the Hopf bifurcations. They divide the different regions of stability to superharmonic disturbances, which are also labelled in the plot according to its character.

To decide whether a time-periodic flow u (obtained by Newton's method) is stable or not we linearize (3.8) around u, as a steady solution for its appropriate $c = L/T$, to obtain the eigenvalues of its Jacobian matrix. If all of the eigenvalues have negative real parts the periodic flow is stable to disturbances of the same wavenumber α but, if there is an eigenvalue with positive real part the solution is unstable. Let us mention that there is always a zero eigenvalue which corresponds to the lack of uniqueness of the time-periodic flow. This is due to the fact that any translation of a rotating wave in the stream direction x, gives rise to the same wave at a different time instant. Indeed, if $u(x, y, 0)$ is the starting position of a rotating wave then, by (4.6), for every $\theta \in \mathbb{R}$ we have $u(x - \theta, y, 0) = u(x, y, \theta/c)$, and thus $u(x - \theta, y, 0)$ lies in the same orbit as $u(x, y, 0)$. In order to achieve uniqueness, we fix one of the coordinates of u by defining a Poincaré section Σ_1. This is given in detail in the next section. The bifurcating diagram for the periodic flows in the Re-A plane together with the stability changes are represented in figure 2. By simply taking a known travelling wave for some α as an initial guess and moving slightly α, we can find periodic solutions for different values of α. These are shown in figure 3, together with their stability.

Now let us discuss the bifurcation diagram shown in figure 3 for $\alpha = 1.02056$. First, the laminar solution becomes unstable at $Re_{cr} = 5772.22$ due to a Hopf bifurcation, that gives rise to a unstable family of periodic orbits. This family continues backwards (with respect to the Reynolds number) until $Re \approx 4660$, when a turning point is reached. Before arriving at this turning point, there is a single eigenvalue of the Jacobian matrix on the real positive axis, while the remaining eigenvalues have negative real part. On traversing through the turning point, a real and negative eigenvalue becomes real positive, so the number of unstable eigenvalues is now two. Shortly after that, these two unstable eigenvalues collide and become a conjugate complex pair (still with positive

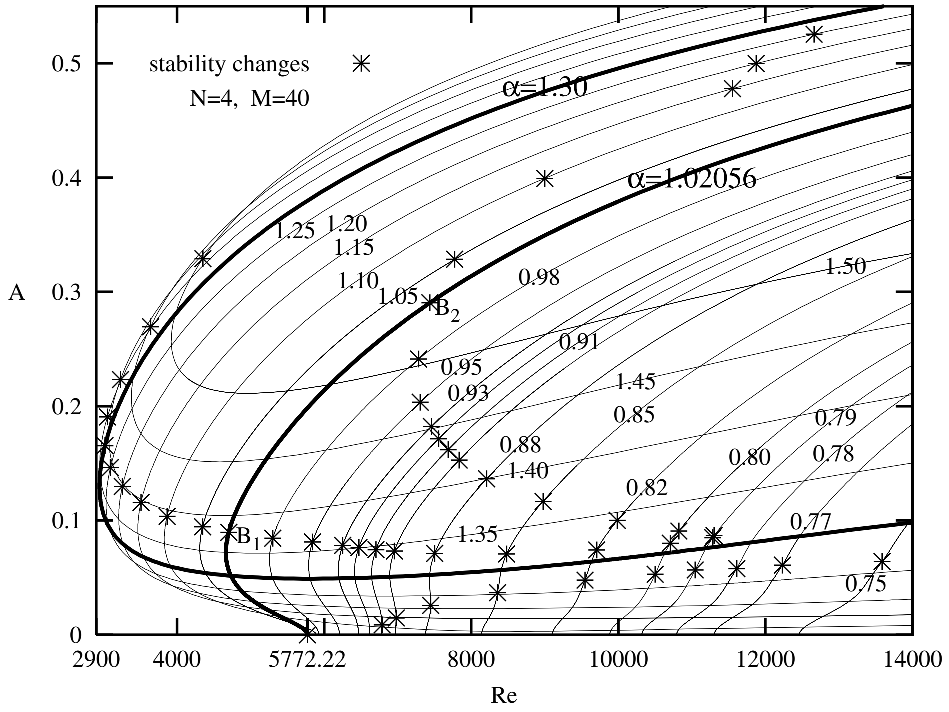

FIGURE 3. Bifurcating curve of periodic flows for several values of α specified on each curve. The number of discretization points is $N = 4, M = 40$. The '*' on each curve have the same meaning as in figure 2. Curves for $\alpha = 1.02056$ and $\alpha = 1.3$ are traced in bigger dots. For $\alpha = 1.02056$ it is attained the critical Reynolds number at $Re = 5772.22$ and for $\alpha = 1.3$ it is approximately reached a solution at a minimum $Re = 2900$.

real part), and then they cross the imaginary axis for $Re \approx 4700$ producing a new Hopf bifurcation at the point B_1 on figure 3. Between $Re \approx 4700$ and $Re \approx 7400$ (at the point B_2 on figure 3), the family of periodic orbits is stable to perturbances of the same wavelength. At $Re \approx 7400$, there is another Hopf bifurcation produced by a conjugate pair of eigenvalues crossing the imaginary axis. These bifurcations persist when M, N (the number of Chebyshev and Fourier modes respectively), are increased and no new ones seem to appear in this range.

Previously, Soibelman & Meiron (1991) found analogous bifurcations for $\alpha = 1.1$, and the critical Reynolds number for which there are time-periodic solutions: $Re \approx 2900$ for $\alpha \approx 1.3$. In figure 3 this minimum Reynolds number is closely attained and even more, there exists an attractor periodic solution for $Re \approx 3000$. For the case of the laminar flow, we obtain the classical results of Orszag (1971) about the critical Reynolds being at $Re_{cr} = 5772.22$. On the one hand, the bifurcation curve of periodic flows reaches the laminar solution at the above mentioned Re_{cr} and in addition, the laminar solution is checked to be stable when $Re < Re_{cr}$ and unstable if $Re > Re_{cr}$. Also we observe that for $\alpha = 1.02056$, it is reached the minimum Reynolds number where the transition from stable to unstable laminar flow takes place, what was formerly presented in figure 1. For $\alpha \gtrsim 1.1$ the curve of periodic solutions does not reach the laminar flow. This is in agreement with the situation in figure 1, since for $\alpha \gtrsim 1.1$ the laminar flow is linearly stable for every Re. In figure 3 we also observe that for $\alpha \gtrsim 0.91$ the curve of periodic flows bifurcates subcritically from the laminar flow, but for $\alpha \lesssim 0.91$ the Hopf bifurcation

N	Re_1	c_1	τ_1	Re_2	c_2	τ_2
			Present work for $\alpha = 1.02056$			
4	4701.7	0.29729	9662.43	7450.1	0.28091	17.93
5	4684.6	0.29881	8983.08	6347.5	0.29014	17.39
6	4686.1	0.29868	9080.07	6355.4	0.29013	17.22
7	4684.1	0.29853	9143.27	6643.2	0.28783	17.33
8	4684.1	0.29857	9125.21	6827.8	0.28608	17.49
			Present work for $\alpha = 1.1$			
4	3864.5	0.31927	7427.55	8946.1	0.26985	17.88
5	3841.0	0.32004	7090.00	7670.3	0.28059	16.87
6	3841.4	0.32018	7065.51	6732.7	0.28927	16.59
7	3840.8	0.32010	7100.30	6844.8	0.28863	16.58
8	3840.6	0.32010	7098.79	7145.8	0.28568	16.75
			Soibelman & Meiron (1991) for $\alpha = 1.1$			
2	3630		4742.32	9400		35.50
3	3800		4935.43	9675		17.65
4	3775		4875.63	9592		16.54

TABLE 1. Convergence of the two first bifurcating Reynolds numbers and associated parameters c and τ for different α. All of them are given for $M = 70$. The values reported in Soibelman & Meiron (1991) for $M = 70$ are also included.

is changed into supercritical and at that point it is born a new Hopf bifurcation on the curve of travelling waves.

Reynolds numbers corresponding to the first two Hopf bifurcations for several values of N are shown in table 1. For the value of $M = 70$, we observe convergence in the results. There are also presented the values obtained from Soibelman & Meiron (1991). For $\alpha = 1.1$ we observe convergence of our results on the first bifurcation as N is increased. Instead, for $N = 8$ we have not yet attained convergence on the second bifurcation. In both cases there are substantial differences with Soibelman & Meiron's (1991) results, being in more agreement for the bifurcation at the lowest Re.

5. Quasi-periodic solutions

In this section, we study the quasi-periodic flows that appear at the Hopf bifurcations of rotating waves found in § 4. For the values of α considered we have obtained different qualitative results than the ones reported in Soibelman & Meiron (1991). For $\alpha = 1.1$ they found that the first Hopf bifurcation to quasi-periodic solutions is subcritical: they obtained quasi-periodic solutions for Re before the bifurcation point. In consequence, close to that point, those bifurcated flows are stable. In the present work, by increasing the number of Fourier modes N, we have achieved a supercritical Hopf bifurcation: the bifurcating quasi-periodic flows are located for Re after the bifurcation point and therefore close to it they are unstable. This is treated in § 5.2. For the second Hopf bifurcation, in agreement with Soibelman & Meiron (1991), the quasi-periodic orbits are found for Re greater than the bifurcation point. More details are given in § 5.1.

We use again the spatio-temporal symmetry of our system. In Rand (1982) it is proved that, with the artificial boundaries of the channel at x and $x + L$, every solution $u(x, y, t)$

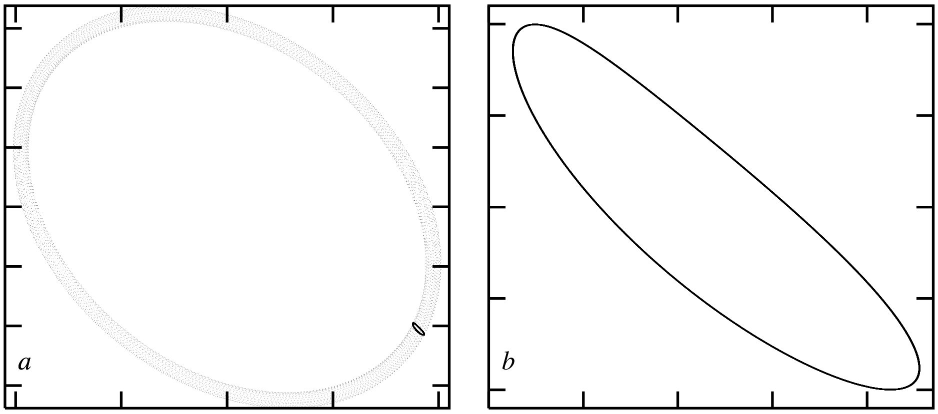

FIGURE 4. Two representations of the solution vector $u(t)$ of a quasi-periodic flow projected on the plane of two selected coordinates namely, $M-1+(2N-3)(M-2)+3$, and $M-1+2(M-2)+5$, for $Re=7509, \alpha=1.02, N=4, M=40$. The range of values for (a) is $[-0.004, 0.004]\times[-0.0008, 0.0008]$ and $[0.0035, 0.0037]\times[-0.0043, -0.0039]$ for (b). In (a) a dot is plotted each $\Delta t = 0.02$ time units. In (b) a dot is plotted only for t when $u(t)\in\Sigma_1$. This last curve is also represented as a reference on the lower right corner of (a).

that lies on an isolated invariant 2-torus (a quasi-periodic solution), not asymptotic to a rotating wave, is a modulated wave, that is to say, there exists $\tau>0$ and $\phi\in\mathbb{R}$ such that

$$u(x, y, n\tau + t) = u(x - n\phi, y, t) \quad \text{for every } n \in \mathbb{Z}. \tag{5.1}$$

As a consequence, this kind of wave has the property that, may be viewed as a τ-periodic wave in a frame of reference moving with speed $c=(pL+\phi)/\tau$, for any integer p. In effect, defining $\tilde{x}=x-ct$ for the previous value of c, and $\tilde{u}(\tilde{x}, y, t)=u(\tilde{x}+ct, y, t)$ as the velocity in the moving frame of reference at speed c, it turns out that

$$\tilde{u}(\tilde{x}, y, \tau) \stackrel{1}{=} u(\tilde{x}+c\tau, y, \tau) \stackrel{2}{=} u(\tilde{x}+pL+\phi, y, \tau) \stackrel{3}{=} u(\tilde{x}, y, 0) \stackrel{4}{=} \tilde{u}(\tilde{x}, y, 0). \tag{5.2}$$

In steps 1, 4 we use the previous definition of $\tilde{u}$. Substituting the value of c we obtain step 2, and because u is L-periodic in x and a modulated wave, one gets step 3. Consequently we have proved that $\tilde{u}(\tilde{x}, y, t)$ is a τ-periodic function of t.

Throughout this section we suppose that $u(t)=(u_1,\ldots,u_K)(t)$ for $K=(2N+1)(M-2)+1$, meaning the real components of what was denoted as $(u_0, \bar{u}_1, \ldots, \bar{u}_N)(t)$ in § 3. In order to look for periodic flows of (5.2), to each value of c we associate a Poincaré section

$$\Sigma_1 = \left\{u \in \mathbb{R}^K \mid u_M = 0\right\},$$

where the flow $u(t)$ is integrated in the Galilean reference at speed c. The selected component u_M, corresponds to the value of $\mathrm{Re}(\bar{u}_1)$ at y_1. Once Σ_1 is defined, we construct a Poincaré map $P_c : \Sigma_1 \longrightarrow \Sigma_1$ as follows: Starting from an initial condition $u=u(0)\in\Sigma_1$ we integrate (3.8), until a time t_c such that $u(t_c)\in\Sigma_1$ for the n_c-th time, where n_c is a positive integer which represents the minimum number of times needed by the flow to return close to the initial point $u(0)$ (the meaning of 'close' will be specified later). We then set $P_c(u(0))=u(t_c)$. In this way we have reduced the search of quasi-periodic flows to a zeros finding problem for the map F defined as

$$0 = F(u, c) \stackrel{\text{def}}{=} P_c(u) - u = u(t_c) - u(0). \tag{5.3}$$

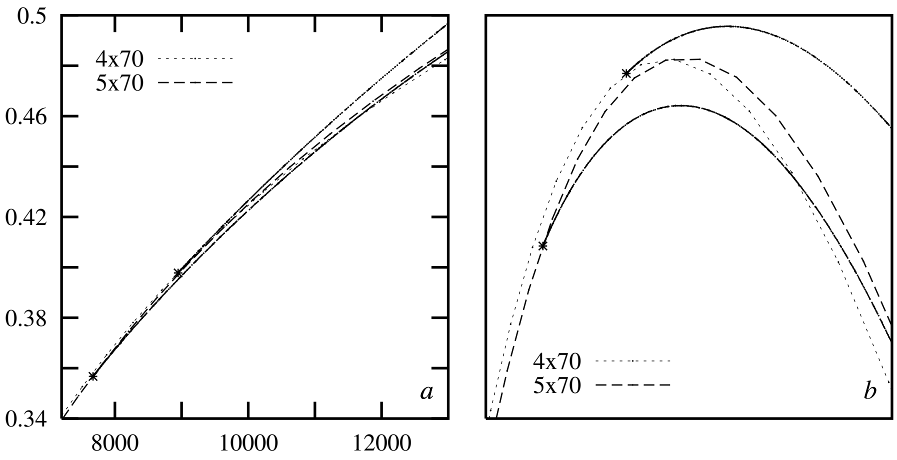

FIGURE 5. (a) Bifurcated branches of quasi-periodic flows at the supercritical Hopf bifurcation of periodic flows at Re_2. Each curve represents A as a function of Re and has specified $N \times M$. Both branches of periodic and quasi-periodic flows are presented. Calculations are shown for $\alpha = 1.1$ and $\Delta t = 0.02$. The '*' correspond to the Hopf bifurcation at Re_2. The bifurcating branch consist of quasi-periodic orbits, stable to disturbances of the same wavenumber. (b) is a clockwise rotation of graph (a).

From (5.1) it is easily checked that, if $P_c(u(0)) = u(t_c) = u(0)$ then $P_c(v(0)) = v(t_c) = v(0)$ for $v(0) = P_0^k(u(0))$ and every positive integer k. Therefore we can generate different points on the same orbit as a solution of (5.3). We avoid this lack of uniqueness by restricting $P_c : \Sigma_1 \cap \Sigma_2 \longrightarrow \Sigma_1$ for

$$\Sigma_2 = \left\{ u \in \mathbb{R}^K \mid u_p = r \right\},$$

and some suitable values of $p \in \mathbb{N}$, $1 \leqslant p \leqslant K$, and $r \in \mathbb{R}$. For Re close to the studied Hopf bifurcations we make $r = u_p(0)$ being $u \in \Sigma_1$ the travelling wave exactly at the bifurcating Re. The selected value of p corresponds to the coordinates $\mathrm{Re}(\bar{u}_N)$ and $\mathrm{Im}(\bar{u}_1)$ of u at $y = 0$, respectively for the first two Hopf bifurcations. If $u(x, y, t)$ is a modulated wave then

$$\int_0^L \int_{-1}^1 u(x,y,\tau)^2 \mathrm{d}y\,\mathrm{d}x = \int_0^L \int_{-1}^1 u(x-\phi,y,0)^2 \mathrm{d}y\,\mathrm{d}x = \int_0^L \int_{-1}^1 u(x,y,0)^2 \mathrm{d}y\,\mathrm{d}x$$

and therefore its amplitude $A(t)$, as defined in (4.8), is a τ-periodic function of t. This is not the case for the rotating waves in figure 2 for which A is constant in time. Thus, in order to consider a concrete value for $A(t)$ in the case of a quasi-periodic flow $u(t)$, we evaluate it at the time t when $u(t) \in \Sigma_1 \cap \Sigma_2$.

We need an initial guess for the Newton's method applied to solve (5.3). We have taken $\alpha = 1.1$ and $M = 70$ as in Soibelman & Meiron (1991), but we have increased the number of Fourier modes using $N \geqslant 3$. According to what was pointed out in § 4 there are two first Hopf bifurcations at $Re_1 \approx 4000$ and $Re_2 \approx 7000$–8000 represented in figure 2 and table 1.

5.1. *Bifurcation at Re_2*

As it was obtained in figure 2, for $Re > Re_2$ the corresponding periodic flow is unstable, so the evolution of (3.8) from such flow as initial condition, drives the fluid away from it. We follow this temporal evolution and observe that the fluid seems to fall in a regular

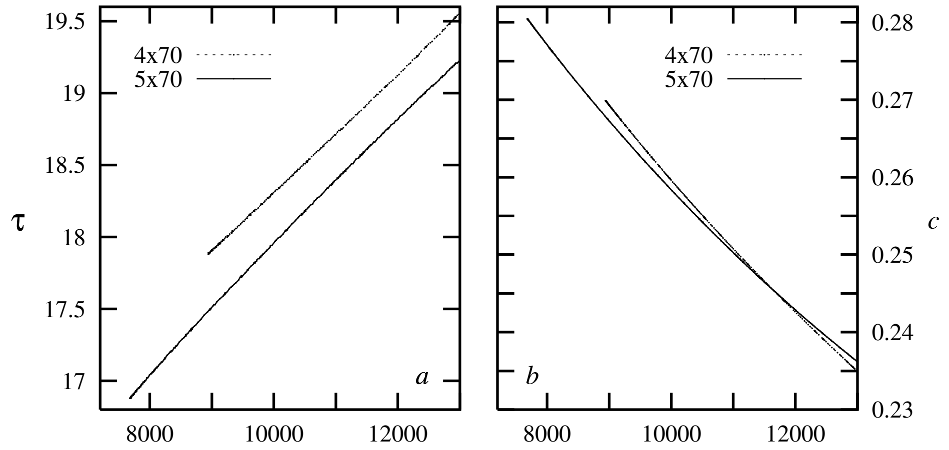

FIGURE 6. Different curves with Re in the abscissa axis, for $N \times M$ points as specified. (a) τ represents the period on time for a quasi-periodic flow when the observer sees it as periodic. (b) The appropriate value of c that converts a quasi-periodic flow in periodic.

régime, which finally proves to be a quasi-periodic attractor solution. This is checked in figure 4 where we plot the projection of the solution vector $u(t) = (u_1, \ldots, u_K)(t)$, over the plane of two arbitrary coordinates (the 120^{th} and 232^{th} say). Each point in figure 4(a) corresponds to the value of the specified coordinates at a time instant. As we can observe, the trajectory seems to fill densely the projection of a 2-torus. Plotting the same coordinates as above, but only when $u(t) \in \Sigma_1$, we see in figure 4(b) a closed curve, which seems to confirm that the flow lives in a 2-torus.

Let us denote as u^0 the attractor 2-torus. We need to approximate the value of c^0 which better makes u^0 appear as a periodic flow. That c^0 exists according to (5.1)–(5.2). We estimate it as (cf. Rand 1982)

$$c^0 = \frac{2\pi}{k} \lim_{t\to\infty} \frac{n(t)}{t}, \quad \text{for} \quad n(t) = \left[\frac{\arg(\overline{u^0_{km}(t)})}{2\pi} \right],$$

where $[\cdot]$ stands for the integer part, k is the number of peaks of the wave u^0 for $x \in [0, L]$ and we have used the midpoint of the channel for $m = M/2$. Next we use u^0, c^0 as the initial condition for Newton's method applied to (5.3) to confirm that our attractor 2-torus u^0 is in fact a modulated wave. Once we have a first point (u^0, Re, c^0) which satisfies (5.3), taking Re as a continuation parameter, we can trace a curve of quasi-periodic flows in the Re–A plane as in § 4 by pseudo-arclength numerical continuation.

As we observe in figure 5, there appears a branch of quasi-periodic solutions which bifurcates from the curve of periodic flows. We emphasize that zeros of $F(c, u)$ can either correspond to stable or unstable quasi-periodic solutions. Since on crossing the bifurcation point Re_2 the periodic orbits go from stable to unstable, the branch of quasi-periodic flows are locally stable to two-dimensional superharmonic disturbances. By means of the eigenvalues of the Jacobian matrix $\partial P_c/\partial u$ we also compute the stability of the obtained quasi-periodic solutions. For the range of $Re \in [7000, 13000]$ studied, all quasi-periodic flows found are stable and the situation is kept when N, M are increased. In figure 6 we present the curves of frequencies c, τ which define the different modulated waves.

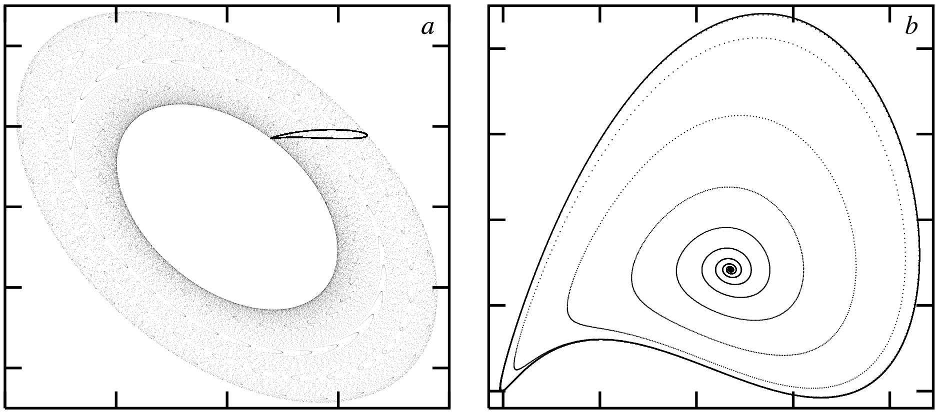

FIGURE 7. Two representations of the solution vector $u(t)$ of a quasi-periodic flow projected on the plane of two selected coordinates for $Re = 3865, \alpha = 1.1, N = 8, M = 70$. The range of values for (a) is $[-0.002, 0.002] \times [-0.001, 0.001]$ and $[0.00037, 0.00129] \times [0.000338, 0.000385]$ for (b). In (a) a dot is plotted each $\Delta t = 0.02$ time units, meanwhile in (b) only for t when $u(t) \in \Sigma_1$. The outer closed curve in (b) is obtained integrating repeatedly for $t \in [0, \tau]$. This curve is also represented as a reference on the right centre of (a).

5.2. *Bifurcation at Re_1*

For $Re < Re_1$ the corresponding time-periodic flow in figure 2 is unstable, but its time evolution ultimately decays to the laminar flow. According to the results in Soibelman & Meiron (1991) concerning with the existence of a subcritical Hopf bifurcation (they take $N \leqslant 2$), we tried to find quasi-periodic flows in the subcritical region, but with no success: we were not able to detect a quasi-periodic attractor solution for $Re < Re_1$ and $N \geqslant 3$. As a consequence we direct the search of quasi-periodic flows to the supercritical region, i.e. for $Re > Re_1$.

It is known from bifurcation theory (see Marsden & McCracken 1976) that in the case of a supercritical Hopf bifurcation in which fixed points before it are unstable and after it stable, the branch of periodic solutions that emanates at the bifurcation point is locally unstable. That should be the situation for $Re > Re_1$ and thus the bifurcating quasi-periodic flows are locally unstable and consequently hard to locate by direct numerical integration, because the evolution of the fluid close to them does not remains near as time evolves.

A good starting guess for the Newton's method applied to (5.3), was searched as follows. First we consider an unstable time-periodic solution $u^P(t)$, i.e. a fixed point of (3.8), for $Re < Re_1$. Next we compute the eigenvalues of the linearization of (3.8) around the fixed point u^P and consider the eigenvector w associated with the most unstable eigenvalue, that is to say, the vector along which the flow escapes in the fastest fashion from u^P. There is just a couple of unstable eigenvalues, which are complex conjugate with positive real part. This is what we expect close to a Hopf bifurcation. Then we integrate numerically the initial condition $u_P(0) + rv$, for $|r| \ll 1$ a small constant, and the direction v is taken in the real plane spanned by the real and imaginary part of w, and thus v is in the plane of most unstable directions. The evolution of the initial condition $u_P(0) + rv$ is carried on until a time when it become as closest as possible to a quasi-periodic flow, according to (5.3) for $Re > Re_1$ following the bifurcation and c near to the one associated with the corresponding periodic orbit for that Re. In this case we

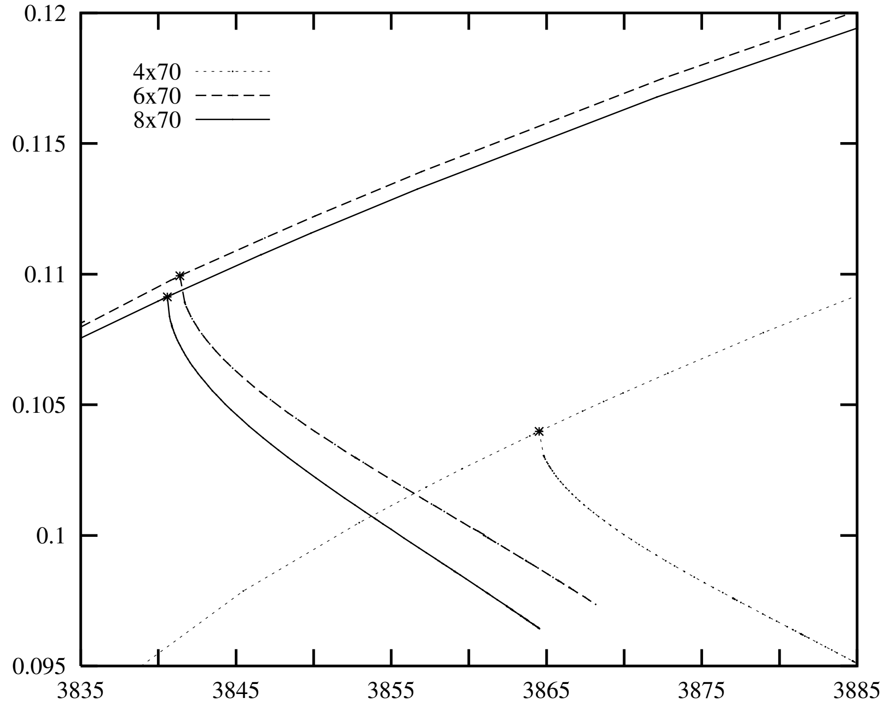

FIGURE 8. Bifurcated branches of quasi-periodic flows at the supercritical Hopf bifurcation of periodic flows at Re_1. Each curve represents A as a function of Re and has specified $N \times M$. Both branches of periodic and quasi-periodic flows are presented. Calculations are shown for $\alpha = 1.1$ and $\Delta t = 0.02$. The '*' correspond to Hopf the bifurcation at Re_1. The bifurcating branch consist of unstable quasi-periodic orbits.

also observe a value of the return time τ of P_c neighbouring to $2\pi/\mathrm{Im}(\lambda)$, being λ the unique purely imaginary eigenvalue (together with its conjugate) at the Hopf bifurcation.

The initial guess obtained in this way is improved through the Newton's method applied to the function $F(u,c)$ defined in (5.3) to finally obtain a first unstable modulated wave for $Re > Re_1$. At this point it is worth to mention the numerical difficulties in evaluating F because the time needed to return to Σ_1 is $\tau \in [7000, 9200]$ as shown in figure 9 for $Re \in [3840, 3885]$. It has been necessary to adapt dynamically the minimum number of times n_c that the solution crosses Σ_1 before it returns to the starting point. For Re close to the Hopf bifurcation n_c starts at 1 and it is incremented by 1 when Re varies approximately in just 2–3 units. When we change slightly Re the return time τ should be varied in accordance. We impose that the new value obtained for τ satisfy $|\tau - \tau_o| < \varepsilon$, for some tolerance ε and τ_o the former return time. If this condition is not fulfilled we increase or decrease n_c by one unit, until it is satisfied.

The approximation of the Jacobian matrix $DF(u,c)$ is implemented by finite differences in which every column is obtained evaluating F in parallel by means of a Beowulf system. This improvement, together with the use of the Broyden's 'good' formula (see Allgower & Georg 1990) in the update of $DF(u,c)$, suppose a substantial increase in the speed of computations.

In figure 7 we present numerical evidence that solutions $u(t)$ of (5.3) lie in a 2-torus and are unstable on time. In a) we observe how the trajectory projected on a plane of two arbitrary coordinates of $u(t)$ fills densely a 2-torus. On the outer curve of b), it is simply

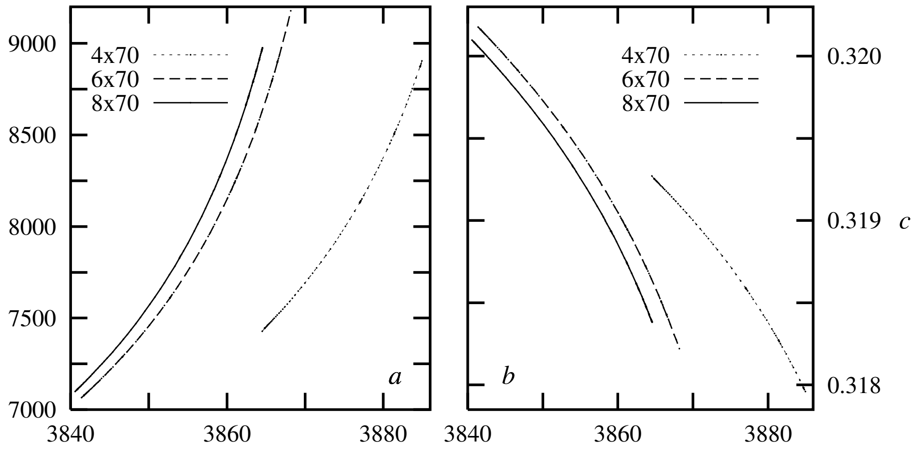

FIGURE 9. Different curves with Re in the abscissa axis for $N \times M$ points as specified. (a) and (b) are as in figure 6.

plotted $u(t)$ when $u(t) \in \Sigma_1$, but if $t > \tau$, being τ is the period of $u(t)$ as a modulated wave, we plot $u(s)$ for s such that $0 \leqslant s = t - p\tau < \tau$ and $p = [t/\tau]$, i.e. we treat $u(t)$ as if it were exactly τ-periodic. We note that, as we are on the Poincaré section, the torus is reduced to a closed curve, which corresponds to the unstable quasi-periodic flow seen as if it were unperturbed. Likewise in b) we let the flow evolve for long time and plot again $u(t)$ when $u(t) \in \Sigma_1$ but suppressing the previous time restriction. Here we can check that the flow is unstable, because it moves away from the outer closed curve and falls to the time-periodic régime: a simple point in the centre of the figure.

Once we have obtained the first solution of (5.3) by the Newton's method, we take Re as a continuation parameter to trace the bifurcating branch of quasi-periodic flows. In figure 8 we plot the amplitude A for each quasi-periodic solution as a function of Re. It seems that we have achieved both qualitative and quantitative convergence because we obtain a similar graph on increasing the values of N, M. It looks also clear from this plot that the Hopf bifurcation is supercritical, so at least locally solutions on the bifurcating branch are unstable. The analysis of the stability of a quasi-periodic solution is done by means of the eigenvalues of the Poincaré map P_c at a fixed point $u(t)$ such that $P_c(u(0)) = u(0)$. In the range of Re presented in figure 8 the quasi-periodic solutions are unstable. Besides, these solutions, unlike the bifurcation at Re_2, present certain symmetry: $\hat{u}_k(y,t)$ is an even or odd function of y depending on the parity of k.

An indicator of the numerical effort involved in the evaluation of the map P_c is plotted in figure 9(a) again for different values of N. The big slope of the Re-τ curve gives rise to high computational cost as Re is increased. Finally in figure 10 the stream lines and levels of vorticity of a quasi-periodic flow are presented, at six equidistant values of time in the interval $[0, \tau]$ for $\tau = 7608.78$.

6. Conclusions

In this work we have studied some bifurcations of plane Poiseuille flow. We have reproduced the results of other authors and obtained similar qualitative results about the Hopf bifurcations, in what concerns to their number and location. The main quantitative differences between Soibelman & Meiron's (1991) computations and ours are due

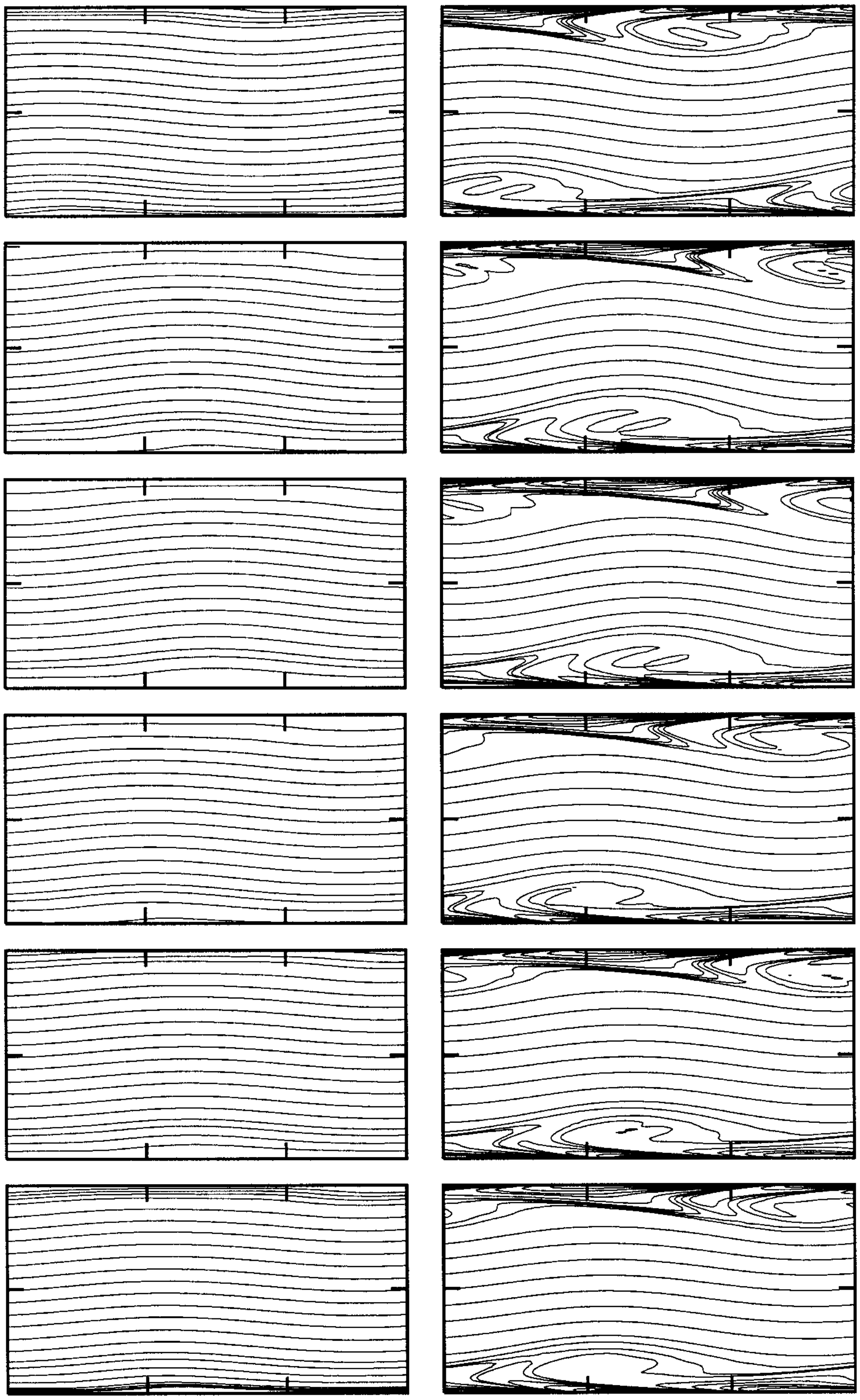

FIGURE 10. Stream lines (left) and levels of vorticity (right) for a unstable quasi-periodic flow at $Re = 3853, \alpha = 1.1, N = 6, M = 70, \Delta t = 0.02$. Surface levels are plotted for $0 \leqslant x \leqslant L, -1 \leqslant y \leqslant 1$. The represented time instants are $0, \tau/6, 2\tau/6, 3\tau/6, 4\tau/6$, and $5\tau/6$ for $\tau = 7608.78$.

to the larger number of points we have used, together with the distinct formulations of the Navier–Stokes equations employed. The important qualitative difference is the kind of bifurcation found at Re_1: in their computations this bifurcation is subcritical, but improving the precision of the numerical approach we obtain that it is supercritical. Then, the bifurcating quasi-periodic orbits are unstable. This has also been confirmed by numerical simulations.

In the case of the bifurcation at Re_1, because the restrictions of long time integration, we have only been able to move away a few tens from Re_1. The further we advanced in Re, the greater are the numerical difficulties we encounter to track the bifurcating branch of quasi-periodic flows, and it is also worth to mention the complications derived from their instability. Close to Re_1 and with the discretization employed ($N = 8$, $M = 70$, $\Delta t = 0.02$), it seems that we have achieved both qualitative and quantitative convergence. By observing figure 8 we can conjecture that, for the range of $\alpha \in [1, 1.1]$ considered, the minimum $Re \approx 2900$ attained with travelling waves is not lowered by quasi-periodic flows. This question still remains open for two-dimensional flows although Ehrenstein & Koch (1991) solved the gap between experiments and numerical results in the case of three-dimensional flows.

For $Re > Re_2$ the quasi-periodic flows encountered are attractor and the integration time is of the order of tens, so in this case the computational cost is drastically reduced compared with the bifurcation at Re_1. The range of Re obtained for attractor flows moves now to several thousands. However, in spite of keeping qualitative convergence, the use of larger Reynolds numbers, makes necessary an increase in precision to get, furthermore, quantitative convergence.

As future work, it would be of interest to know whether those two groups of quasi-periodic flows bifurcate into other class of more complicated solutions: a new vortical state which could approach more the transition to turbulence. In the interval of Re analysed we have not detected any change of stability: bifurcated solutions at Re_1 are always unstable, meanwhile at the bifurcation in Re_2 they are stable. For the stable solutions we have only consider disturbances with the same wavenumber α.

We thank C. Simó and J. Solà-Morales for valuable discussions during the preparation of this paper. This research has been partially supported by funds from the Departamento de Matemática Aplicada I (Universidad Politécnica d e Cataluña), the Spanish grant CICYT BFM2000–0623, the Catalan grant CIRIT 2000SGR–00027, and DURSI. The computing facilities of the UB-UPC Dynamical Systems Group (clusters Hidra and Eixam) have been widely used.

REFERENCES

ALAVYOON, F., HENNINGSON, D. S. & ALFREDSSON, P. H. 1986 Turbulent spots in plane Poiseuille flow – flow visualization. *Phys. Fluids* **29**, 1328–1331.

ALLGOWER, E. L. & GEORG, K. 1990 *Numerical Continuation Methods*, *Springer Series in Computational Mathematics*, vol. 13. Springer-Berlag.

CANUTO, C., HUSSAINI, M. Y., QUARTERONI, A. & ZANG, T. A. 1988 *Spectral methods in fluid dynamics*. Springer-Verlag.

CARLSON, D. R., WIDNALL, S. E. & PEETERS, M. F. 1982 A flow visualization study of transition in plane Poiseuille flow. *J. Fluid Mech.* **121**, 487–505.

DRISSI, A., NET, M. & MERCADER, I. 1999 Subharmonic instabilities of Tollmien-Schlichting waves in two-dimensional Poiseuille flow. *Phys. Rev. E* **60** (2), 1781–1791.

EHRENSTEIN, U. & KOCH, W. 1991 Three-dimensional wavelike equilibrium states in plane Poiseuille flow. *J. Fluid Mech.* **228**, 111–148.

HERBERT, T. 1976 Periodic secondary motions in a plain channel. In *Proc. 5th Intl. Conf. on*

Numerical Methods in Fluid Dynamics, *Lecture Notes in Physics*, vol. 59, pp. 235–240. Springer.

Herbert, T. 1991 Exploring transition by computer. *Appl. Num. Maths* **7**, 3–25.

Jiménez, J. 1987 Bifurcations and bursting in two-dimensional Poiseuille flow. *Phys. Fluids* **30** **(12)**, 3644–3646.

Jiménez, J. 1990 Transition to turbulence in two-dimensional Poiseuille flow. *J. Fluid Mech.* **218**, 265–297.

Marsden, J. E. & McCracken, M. 1976 *the Hopf bifurcation and Its Applications*, *Applied Mathematical Sciences*, vol. 10. Springer.

Maslowe, S. A. 1985 *Shear flow instabilities and transition*, *Topics in applied physics*, vol. 45, chap. 7, pp. 181–228. Springer-Verlag.

Nishioka, M. & Asai, M. 1985 Some observartions of the subcritical transition in plane Poiseuille flow. *J. Fluid Mech.* **150**, 441–450.

Orszag, S. A. 1971 Accurate solution of the Orr–Sommerfeld stability equation. *J. Fluid Mech.* **50–4**, 689–703.

Pugh, J. D. & Saffman, P. G. 1988 Two-dimensional superharmonic stability of finite-amplitude waves in plane Poiseuille flow. *J. Fluid Mech.* **194**, 295–307.

Rand, D. 1982 Dynamics and symmetry predictions for modulated waves in rotating fluids. *Arch. Rat. Mech. Anal.* **79**, 1–37.

Rozhdestvensky, B. L. & Simakin, I. N. 1984 Secondary flows in a plane channel: their relationship and comparison with turbulent flows. *J. Fluid Mech.* **147**, 261–289.

Saffman, P. G. 1983 Vortices, stability, and turbulence. *Ann. N. Y. Acad. Sci.* **404**, 12–24.

Soibelman, I. & Meiron, D. I. 1991 Finite-amplitude bifurcations in plane Poiseuille flow: two-dimensional Hopf bifurcation. *J. Fluid Mech.* **229**, 389–416.

Squire, H. B. 1933 On the stability of the three-dimensional disturbances of ivscous flow between parallel walls. *Proc. Roy. Soc. London Ser. A* **142**, 621–628.

Thomas, L. H. 1953 The stability of plane Poiseuille flow. *Phys. Rev.* **91** (4), 780–783.

Zahn, J.-P., Toomre, J., Spiegel, E. A. & Gough, D. O. 1974 Nonlinear cellular motions in Poiseuille channel flow. *J. Fluid Mech.* **64**, 319–345.